Astron. Astrophys. 357, 7–12 (2000)

ASTRONOMY AND ASTROPHYSICS

VLBA H I absorption observations of the water megamaser galaxy NGC 5793

Y.M. Pihlström[1], **J.E. Conway**[1], **R.S. Booth**[1], **P.J. Diamond**[2], **and B.S. Koribalski**[3]

[1] Onsala Space Observatory, 439 92 Onsala, Sweden
[2] MERLIN/VLBI National Facility, Jodrell Bank Observatory, Macclesfield, Cheshire, SK11 9DL, UK
[3] Australia Telescope National Facility, CSIRO, P.O. Box 76, Epping NSW 2121, Australia

Received 6 May 1999 / Accepted 17 February 2000

Abstract. We report parsec-scale resolution observations of neutral hydrogen seen in absorption in the $\lambda = 21$ cm line in the H_2O megamaser galaxy NGC 5793. We find that the total H I column density of $5 \times 10^{22} (\frac{T_{\rm sp}}{100\,{\rm K}})\,{\rm cm}^{-2}$ is divided into three narrow (FWHM $\leq 16\,{\rm km\,s}^{-1}$) and one broad component (FWHM $50\,{\rm km\,s}^{-1}$). The narrow components have H I column densities of $\sim 5 \times 10^{21} (\frac{T_{\rm sp}}{100\,{\rm K}})\,{\rm cm}^{-2}$ and there is evidence that they have sizes $\simeq 15$ pc and H I densities of $\sim 150 (\frac{T_{\rm sp}}{100\,{\rm K}})\,{\rm cm}^{-3}$. The broad absorption component shows a velocity gradient in the same direction as the CO disk observed in this source. We argue that this broad component could be due to a circumnuclear disk or torus. The observed velocity gradient implies that this structure has radius $\sim$ 50–100 pc.

Key words: galaxies: active – galaxies: individual: NGC 5793 – galaxies: ISM – radio lines: galaxies

1. Introduction

Recently, numerous observations have shown disk-like distributions of gas in the central (< 1 kpc) parts of active galactic nuclei (AGN), e.g. HST imaging of NGC 4261 (Jaffe et al. 1993). This gas probably has a role in both feeding the central AGN and in blocking the direct view of the central engine from some directions; hence forming the basis of the orientation-based unified schemes. In the radio regime the small angular scales on which this gas occurs requires VLBI techniques to resolve its spatial distribution. From such observations important physical properties like the enclosed mass may be derived, e.g. from H_2O megamasers in NGC 4258 (Miyoshi et al. 1995), or from H I absorption in Cyg A (Conway 1998). In addition such observations can reveal the density and temperature of the circumnuclear gas and whether it is molecular, atomic or even ionised.

NGC 5793 is an optically bright spiral galaxy at a distance of 70 Mpc (we use H_0=50 km s^{-1} Mpc^{-1} throughout this paper) with an inclination of 73°. Optical emission line diagnostics identify this source as a Seyfert 2 galaxy (Baan et al. 1998). Amongst its unusual AGN-like properties it harbours a strong (~ 1 Jy) relatively compact (< 80 mas) radio source. This source also shows water masers at velocities $\pm 250\,{\rm km\,s}^{-1}$ around the optical systemic velocity (Hagiwara et al. 1997), and the same observations tentatively detect weaker maser features at the systemic velocity. In its H_2O maser properties this source is therefore very similar to NGC 4258 where the satellite and systemic velocity lines arise due to an edge-on molecular disk of inner radius 0.13 pc in Keplerian rotation about a 3.5×10^7 $M_\odot$ mass black hole (Miyoshi et al. 1995). Furthermore NGC 5793 is remarkable in that it possesses H I absorption of very large opacity ($\tau > 2$) over a relatively wide velocity width (FWHM $\sim 100\,{\rm km\,s}^{-1}$, Fig. 1). Associated with this H I absorption is much lower opacity OH absorption (Gardner & Whiteoak 1986). Even though there is no H I emission detected on VLA scales (Gardner & Whiteoak 1986), NGC 5793 has a disk-like structure detected in CO(J=1-0) emission that extends out to a radius of ~ 1.6 kpc (Hagiwara et al. 1997, Hagiwara 1998).

In other objects, which show wide velocity H I absorption, there is clear evidence that the H I absorbing gas is associated with the AGN (Conway 1998; Gallimore et al. 1998; Koribalski 1996; Pedlar et al. 1996). It is therefore interesting to study NGC 5793 to see whether the very high opacity H I absorption in this object is related to the compact H_2O maser emitting disk that presumably exists, or whether it occurs on larger radii (a few hundred pc) as appears to be the case for several nearby Seyferts (Gallimore et al. 1999). Previous low resolution VLBI H I absorption observations of NGC 5793 were made by Gardner et al. (1992) and left the nature of the H I absorption unclear - here we report on much higher spatial and spectral resolution observations using the VLBA.

2. Observations and results

2.1. Observational details

The new 21 cm H I absorption observations were made in December 1996 and used the 10-element VLBA centred at the redshifted frequency of 1404 MHz. A bandwidth of 4 MHz (correlated with 512 channels) corresponding to $850\,{\rm km\,s}^{-1}$ covered the range of known absorption centred at the optical redshift of the galaxy ($cz = 3491 \pm 66\,{\rm km\,s}^{-1}$, heliocentric

Send offprint requests to: Y.M. Pihlström (ylva@oso.chalmers.se)

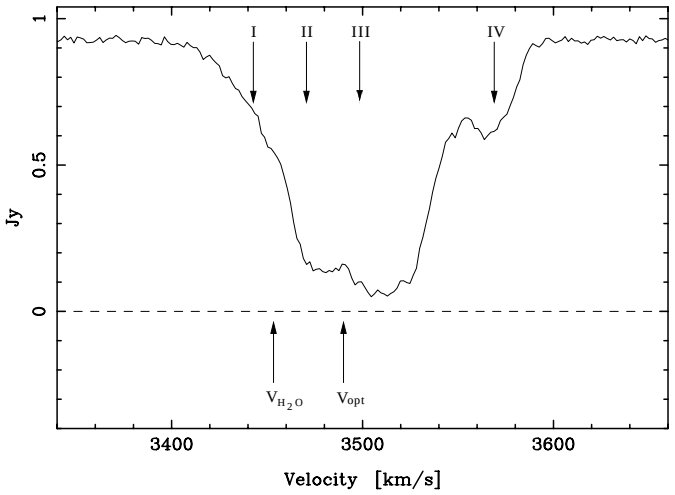

Fig. 1. Total neutral atomic hydrogen absorption averaged over the whole continuum. The upper arrows mark the velocity centroids of the four different spectral features (see Fig. 4). The two bottom arrows mark the optical systemic velocity and the velocity centroid of the systemic water maser features respectively

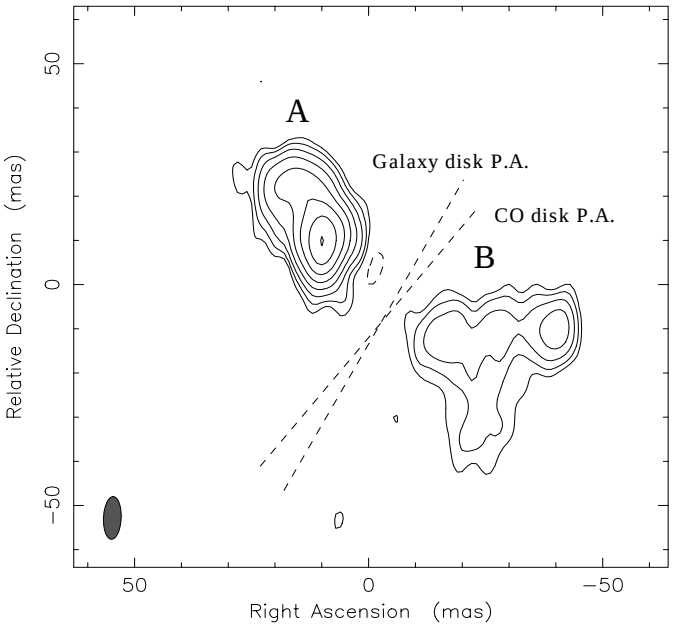

Fig. 2. 1.4 GHz continuum map of NGC 5793 with contours at (1, 2, 4, 8, 16, 32, 64 and 128)$\times 2.47$ mJy/beam. The map peak intensity is 325 mJy/beam. The north-east and the south-west continuum structures are labelled A and B respectively. At a distance of 70 Mpc ($H_0 = 50\,\mathrm{km\,s^{-1}\,Mpc^{-1}}$) 1 mas corresponds to 0.34 pc. The dotted lines indicates the major axis of the host galaxy disk ($-30°$) and of the CO disk ($-40°$) respectively

frame and optical velocity convention). The on-source integration time was 6.4 hrs and every hour one 20 minute scan of a calibrator was included. Initial data reduction including bandpass calibration was carried out using standard tasks in AIPS. A set of line-free continuum channels was then selected on either side of the very deep absorption line, averaged and used to create a continuum map within DIFMAP (Fig. 2). The spectral line data were amplitude- and phase-calibrated against this continuum map, the continuum subtracted using UVLIN, and the data were smoothed in frequency to give $3.3\,\mathrm{km\,s^{-1}}$ spectral resolution and then mapped. For the high spatial resolution, uniformly weighted, spectral cube the rms noise in each channel was 2.5 mJy/beam, while in the continuum map the rms noise was 0.5 mJy/beam. Finally a cube of optical depth (τ) was created within AIPS.

2.2. Results

As seen from Fig. 2, the parsec-scale radio continuum structure is somewhat different from the core-jet structure normally found in bright AGN. The location of the nucleus is unclear; it may be associated with the continuum peak, lie between the two main continuum components or be associated with the linear east-west structure within the south-west component. More detailed investigations of the spectral indices for different components are needed to find the core location. Hereafter we will refer to the north-east continuum component as A, and the south-west structure as B.

Fig. 1 shows the integrated absorbed flux over the whole VLBI source, and confirms the results of Gardner et al. (1992) who found a complex absorption line consisting of several components separated in velocity. Two position-velocity diagrams were constructed along the major axes of the two continuum structures respectively (Fig. 3a and b.); over component A along P.A. = $30°$ and over B along P.A. = $90°$.

To find any further spatial variations of the different spectral features optical depth spectra were taken towards the continuum at six different positions (Fig. 4). In order to parameterise the opacities and linewidths of the spectral components Gaussians were fitted to each of the spectra (dashed lines in Fig. 4). We found that a minimum of four Gaussians were required to adequately fit the data; we refer to these as I, II, III and IV in order of increasing centroid velocity (marked in Fig. 1). The four features fit the data well over component A. Given the lower SNR of the data over B we fitted these spectra starting with the same four Gaussians fitted to A. This strategy also allows a direct comparison between the spectra at the two continuum components.

Table 1 lists the location at which the opacity of each of the spectral features (I-IV) peaks. The FWHM, peak opacity and velocity centroid are also listed as well as the column density of H I derived assuming a spin temperature $T_{\rm sp}$ of 100 K and a covering factor of unity. The total H I column density is found to be $5 \times 10^{22} (\frac{T_{\rm sp}}{100\,K})\,\mathrm{cm^{-2}}$. We find no significant variation of the FWHMs of the spectral features I, II and IV across the source. In contrast, feature III varies in its FWHM with wider values found over B. However we note that this might be an artifact due to ambiguities in the relative strength of features II and III over B. As seen from Fig. 3a and b. no significant velocity gradients are present over A. In contrast a velocity gradient of $1.3 \pm 0.4\,\mathrm{km\,s^{-1}/pc}$ is indicated over B. It is apparent (Fig. 4)

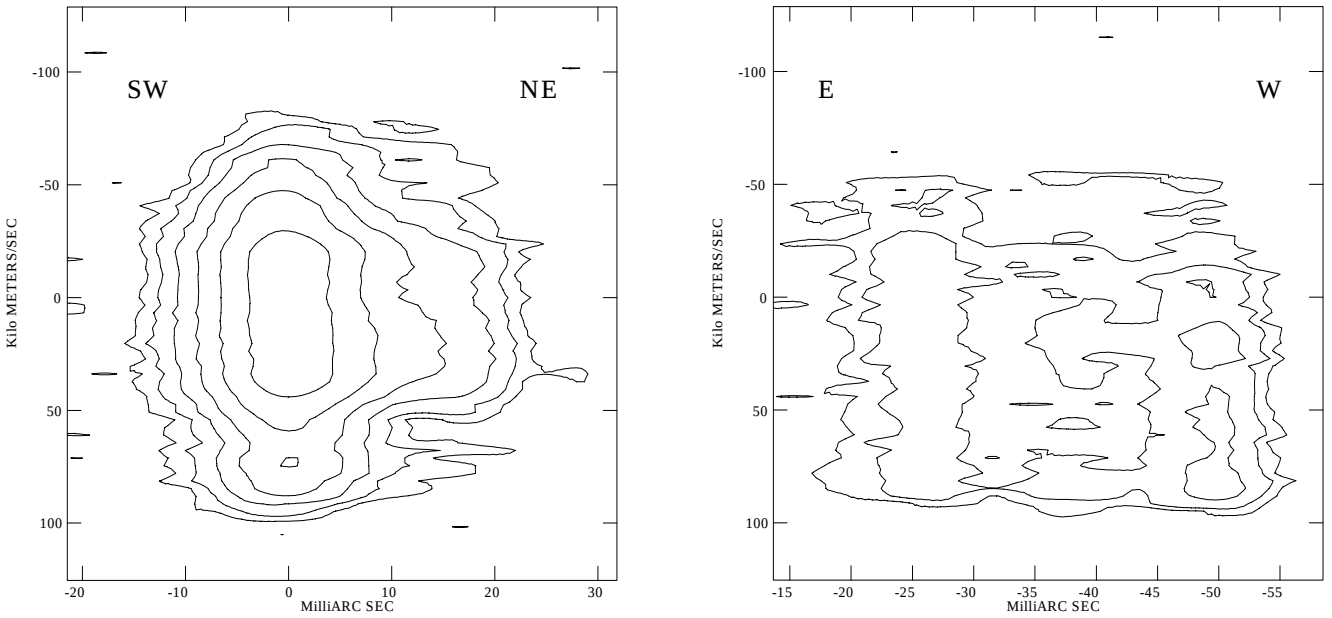

Fig. 3a and b.. Position-velocity diagrams of the absorbed H I flux density. Zero position refers to the location where the continuum emission peaks, while zero velocity is referenced to the optical velocity at 3491 km s^{-1}. Plotted contours are 7.5, 15, 30, 60, 120 and 240 mJy/beam. **a** Component A rotated 30°, which should reveal velocity gradients along the major axis of A in the direction northeast-southwest **b** Component B with no rotation, following an east-west line

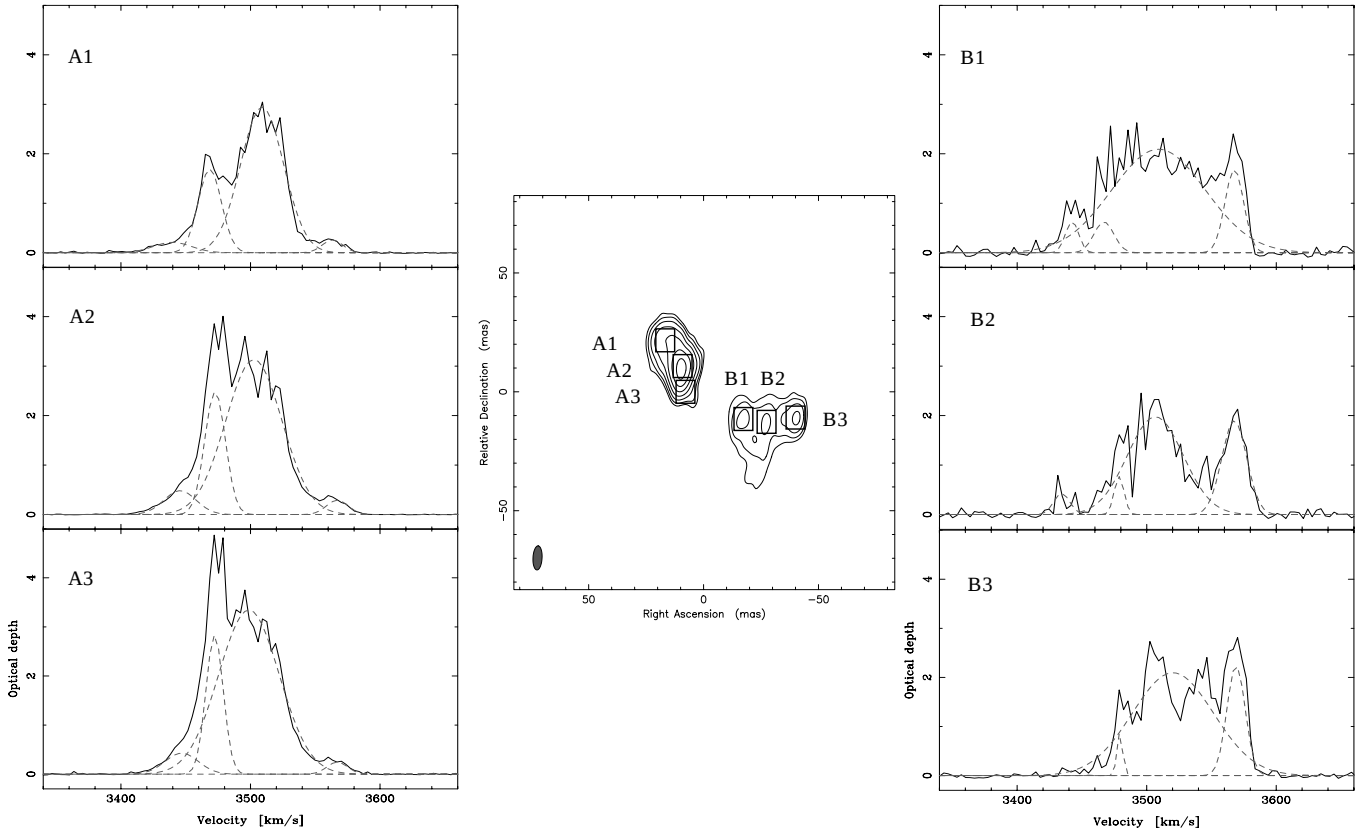

Fig. 4. Side panels show optical depth spectra at six different locations (A1 to B3). The positions of these regions on the continuum source is shown in the middle panel. Dashed lines show the individual Gaussian components (named I-IV in order of increasing centroid velocity, see Sect. 2.2) fitted to each of the spectra

Table 1. Parameters of the four spectral features at the positions where their opacities peak.

Feature	Peak opacity at component	Peak opacity	FWHM [km s^{-1}]	$N_{HI}(\frac{T_{sp}}{100\,K})^{-1}$ [cm^{-2}]	Velocity [km s^{-1}]
I	B1	0.7 ± 0.1	12 ± 1.0	$1.5 \pm 0.3 \times 10^{21}$	3442 ± 0.4
II	A3	2.7 ± 0.2	16 ± 0.1	$7.1 \pm 0.6 \times 10^{21}$	3472 ± 0.3
III	A3	3.4 ± 0.2	54 ± 0.2	$3.5 \pm 1.8 \times 10^{22}$	3499 ± 0.1
IV	B3	2.2 ± 0.6	16 ± 0.3	$6.7 \pm 1.7 \times 10^{21}$	3569 ± 5.6

that the E-W velocity gradient over B is mainly due to a change in the velocity centroid of the broad feature III. Comparing the centroid velocity of III at A and B respectively, we find a shift of 1.2 ± 0.4 km s^{-1}/pc, which is consistent with the above velocity gradient continuing beyond B.

Fig. 5 plots the column densities of the spectral features (I-IV) over each of the spatial components A1-B3. This plot shows for each spectral feature the change in column density following a ridge-line over the continuum that starts in the north-east part of A and ends at the most western part of B.

2.3. Cloud sizes, densities and spin temperatures

Our results (Sect. 2.2) show that the total H I absorption toward the nucleus, with column density $5 \times 10^{22}(\frac{T_{sp}}{100\,K})$ cm^{-2}, is divided into a broad (feature III) and three narrower features (I, II and IV) each with column densities $\sim 5 \times 10^{21}(\frac{T_{sp}}{100\,K})$ cm^{-2}. Fig. 5 shows that the low opacity parts of the spectral features are extended; however we can make a first order estimate of the sizes of any associated cloud. The best example is feature II, which has a maximum in its column density at locations A2 and A3. The data shown in Fig. 4 and Fig. 5 are consistent with spectral feature II being due to a cloud of FWHM 16 km s^{-1} and size 15 pc. Assuming a covering factor of unity we find a H I column density of $7 \times 10^{21}(\frac{T_{sp}}{100\,K})$ cm^{-2}; $n_{HI} = 150(\frac{T_{sp}}{100\,K})$ cm^{-3} and assuming a spherical cloud shape a total atomic hydrogen mass of $\sim 7 \times 10^3(\frac{T_{sp}}{100\,K})$ M$_\odot$. We will conservatively estimate the H I kinetic temperature to be $\simeq 100$ K, similar to cool neutral H I in the Galaxy.

2.4. Associated OH absorption

Gardner & Whiteoak (1986) found that in NGC 5793 the OH 1667 MHz absorption is associated in velocity with the H I absorption. To make a quantitive comparison of H I and OH absorption for each of our spectral components we compare our opacity spectra averaged over the whole source (Fig. 1) with the VLA OH spectra of Gardner & Whiteoak (1986). At a first glance the OH absorption appears much narrower than the H I, but the strong resemblance of the shape of the two higher velocity absorption features (our features III and IV) suggests a direct connection between OH and H I. Moreover the similar FWZI of the OH and H I lines is consistent with each of the spectral features (I-IV) seen in H I being present in OH, but feature II being much weaker in OH. This lower OH abundance for feature II then explains the apparently narrower OH line shape. Alternatively these lower velocity absorbing gas systems may simply have no association in OH and H I. Higher spectral resolution observations of the OH in comparison with our H I are needed to determine if the low velocity OH and H I are connected.

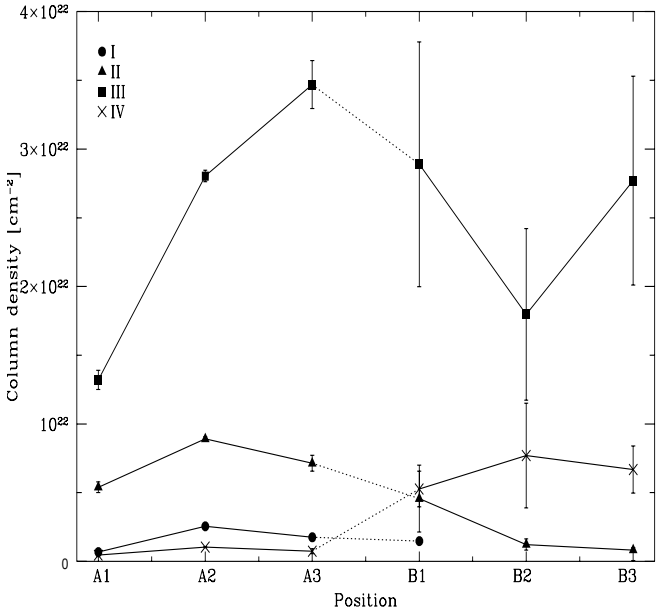

Fig. 5. The apparent H I column density distributions (assuming $T_{sp} = 100$ K and a uniform covering factor) of the four spectral features (I-IV). Plotted is column density as a function of location across the VLBI source. The dotted lines represent an interpolation between the two continuum structures A and B. The errorbars are plotted at the one sigma level

Table 2 lists OH and H I opacities and column densities for features I-IV, and the ratios τ_{OH}/τ_{HI} and N_{OH}/N_{HI} assuming all of the OH and H I features to be related. The column densities of H I were computed using linewidths from Table 1 and assuming a spin temperature of $T_{sp} = 100$ K. NGC 5793 is a strong IR source (Surace et al. 1993) and for the expected gas densities the OH excitation temperature is likely to be determined by coupling to this IR radiation field rather than collisions. Given the observed IR luminosity we calculated an OH excitation temperature ~ 30 K for gas at $r \sim 200$ pc.

For spectral features I, III and IV (Fig. 1) the VLA OH and H I spectra strongly resemble each other with an opacity ratio of 0.024; while at the velocity corresponding to feature II, the line ratio and estimated N_{OH}/N_{HI} is almost three times smaller. In features I, III and IV we find values for N_{OH}/N_{HI} to be of the order of 9×10^{-7}. The models of X-ray irradiated circumnuclear

Table 2. Comparison of H I and OH properties.

Feature	$\tau_{\rm OH}$	$\tau_{\rm HI}$	$\frac{\tau_{\rm OH}}{\tau_{\rm HI}}$	$N_{\rm OH}(\frac{T_{\rm ex}}{30\,K})^{-1}$ [cm^{-2}]	$N_{\rm HI}(\frac{T_{\rm sp}}{100\,K})^{-1}$ [cm^{-2}]	$\frac{N_{\rm OH}}{N_{\rm HI}}$
I	0.0063	0.244	0.026	5.2×10^{14}	5.3×10^{20}	9.8×10^{-7}
II	0.0158	1.711	0.009	1.7×10^{15}	5.0×10^{21}	3.4×10^{-7}
III	0.053	2.222	0.024	1.9×10^{16}	2.2×10^{22}	8.6×10^{-7}
IV	0.0147	0.622	0.024	1.6×10^{15}	1.8×10^{21}	8.9×10^{-7}

gas presented by Maloney et al. (1996) predict such an OH/H I ratio for gas which is approximately equally atomic and molecular (NGC 5793 is known to harbour an X-ray source; Tashiro M., private comm.). Given the OH and H I absorption we therefore argue that the total column density of gas in NGC 5793 lies somewhere between 5×10^{22} cm^{-2} and a few times this value. Such column densities are comparable to these traced by X-ray photoelectric absorption in Seyfert 2s (Risaliti et al. 1999).

The ratio $N_{\rm OH}/N_{\rm HI}$ for features I, III and IV is at least ten times larger than that found in diffuse molecular clouds in the Galaxy ($1 - 3 \times 10^{-8}$, Liszt & Lucas 1996). On the other hand the OH/H I ratio is about a factor of 10 *less* than that found in other galaxies showing both OH and H I in absorption. For instance, VLA H I and OH absorption observations of the SBa galaxy NGC 660 (Baan et al. 1992) have revealed a rotating disk with an inner radius of 160 pc, which shows a $N_{\rm OH}/N_{\rm HI}$ ratio $\sim$ 4–10×10^{-6} (using the same excitation temperatures as for NGC 5793) which is an order of magnitude larger than what we find in NGC 5793. Similarly, the Sbc galaxy NGC 3628 shows a rotating disk both in OH and H I absorption, where OH/H I is ten times larger than in NGC 5793 (Schmelz et al. 1987).

2.5. Relation to H_2O maser emission

Based on the information provided by Hagiwara et al. (1997) we convert the H_2O velocities to a heliocentric, optical definition frame. We then find that the two satellite water masers occur at 3164 and 3640 km s^{-1} respectively, clearly offset from the H I absorbing velocities (3410–3590 km s^{-1}, see Fig. 1). However in addition Hagiwara et al. (1997) found evidence for weak systemic velocity H_2O masers between 3370 and 3526 km s^{-1}. We estimate a characteristic centroid velocity of 3455 km s^{-1} for these masers, which lies somewhere between our feature I ($V_{\rm II} = 3442$ km s^{-1}) and feature II ($V_{\rm II}$=3472 km s^{-1}).

3. Discussion

An important issue is whether the H I absorbing clouds we detect are a part of a structure which feeds and hides the AGN, or are instead unrelated clouds in the ISM of the host galaxy. A closely related problem is their distance from the central engine of the AGN. In the following we discuss alternative locations for the absorbing gas.

3.1. Connection with the H_2O masers

The H I clouds could be relatively close to the nucleus, perhaps just outside the proposed H_2O megamaser rotating disk (Hagiwara et al. 1997). It has been argued in NGC 4258 for instance (Neufeld & Maloney 1995), that atomic gas should lie immediately outside the water maser emitting circumnuclear disk on scales $r < 10$ pc.

The H_2O masers in NGC 5793 have similar satellite lines to NGC 4258, and so H I gas would be expected on similar scales in this object. The fact that we see H I absorption over all VLBI continuum components, i.e. extended over 30 pc - obviously argues against all of the H I gas being associated with the outer parts of a compact H_2O disk at $r < 10$ pc. However, it is important to keep in mind that different H I spectral features might occur at different distances from the AGN. This seems to be the case in our own Galactic centre where one of the H I absorption features might be associated with the CND while others are more distant from the centre (Liszt et al. 1983). In NGC 5793 it is plausible that one of the low velocity features I or II, which are the ones closest in velocity to the systemic H_2O masers and which are located principally over component A, lie very close to the central engine (< 10 pc). The different OH/H I ratio found for feature II could in this case be explained by a larger X-ray ionisation parameter which reduces the gas molecular fraction (Maloney et al. 1996). In addition the presence of a very strong nearby radio continuum source could depress the OH 18 cm absorption due to radiative excitation effects (Black 1998). In contrast, if the H I density is high enough ($\sim 10^4$ cm^{-3}) its spin temperature at $r = 10$ pc will remain at a few hundred K, thus giving high H I opacity.

3.2. Normal ISM clouds

Due to the complete coverage of the VLBI source (> 30 pc), the bulk of the H I absorbing gas must be situated much further away from the nucleus than any presumed water maser emitting disk. However, given the total column densities of 5×10^{22} cm^{-2} which are much larger than in the disk of our own Galaxy, it seems unlikely that the gas would simply be due to gas in the normal ISM of the host galaxy. Such substantial column densities are instead comparable to column densities toward Seyfert 2 nuclei (Risaliti et al. 1999). Moreover, the velocity widths of the spectral features in NGC 5793 (15–50 km s^{-1}) are significantly broader than in the Galaxy outside our Galactic circle (~ 5 km s^{-1}, Dickey et al. 1978, Mebold et al. 1981).

3.3. Randomly moving clouds or circumnuclear torus?

Given the detection of a CO-disk of radius 1.6 kpc in NGC 5793 (Hagiwara 1998), it would be more natural to assume that the

H I arises within this 1.6 kpc region. Assuming that the H I gas is cospatial with the CO, the rotation velocity of the CO disk (225 km s^{-1}, Hagiwara et al. 1998) implies however an undetectable velocity gradient across B of 0.1 km s^{-1}/pc. Instead, for spectral feature III we find a larger observed gradient of 1.3 km s^{-1}/pc (Sect. 2.2). It follows that if the apparent velocity gradient over B, in addition to the shift between A and B, is due to systematic rotation then the H I is much closer to the centre than the CO. It is, of course, possible that the gradients are simply random velocity fluctuations due to overlapping clouds; and that the different velocity features are just randomly radially infalling or outflowing H I gas clouds. However arguing for rotation is the consistency of the velocity gradient both over B and between A and B. This is backed up by the fact that we see a velocity gradient across B but not along A. Both behaviours are consistent with the velocity gradient being due to rotation in the plane defined by the CO- or galaxy-disk (see Fig. 2). Assuming the H I gas has the same inclination as the optical galaxy (73°) then the gradient between A and B for feature III implies that $V_{rot}/r = 3.3$ km s^{-1}/pc, where r is the radius of the disk and V_{rot} is the rotation velocity. Similar ratios are found for the disks in the Seyferts modelled by Gallimore et al. (1999). In these objects a rotation velocity of a few hundred km s^{-1} is common; applying $V_{rot} = 200$ km s^{-1} the H I gas in NGC 5793 would be found at $r = 60$ pc.

If we accept that the bulk of H I absorption found in feature III occurs at $r = 50$–100 pc then the absorption occurs on similar scales as in other Seyfert 2s (Gallimore et al. 1999). The broad H I could therefore be part of an extended continuous torus or disk structure which feeds the central engine. The unusually high opacity may then simply be due to the high inclination of the disk so that the line of sight probes a significant amount of gas. Spectral features I, II and IV could in this scenario be due to individual H I clouds interior or exterior to the main H I circumnuclear torus.

4. Summary

Although from our H I VLBI data alone it is not possible to unambiguously determine how far this atomic gas is from the galaxy centre, the bulk of the gas is not immediately connected to the H_2O maser emitting disk that is presumed to occur a few parsecs radius from the central nucleus. Moreover, the large total column densities imply that is not likely that the gas is just normal ISM clouds in the host galaxy and hence unrelated to the AGN phenomenom. The velocity gradient detected for the broad H I absorption feature III is in the same direction and sense as the CO disk at $r = 1.6$ kpc and suggests that this feature is due to circumnuclear gas. The higher velocity gradient from the H I implies that the H I lies much closer ($r \sim 50$–100 pc) to the nucleus.

Acknowledgements. We wish to thank the referee for useful suggestions and comments on the manuscript.

References

Baan W.A., Rhoads J., Haschick A.D. 1992, ApJ 401, 508
Baan W.A., Salzer J.J., Lewinter R.D. 1998, ApJ 509, 633
Black J.H. 1998, In: Hartquist T.W, Williams D.A. (eds.) The molecular Astrophysics of Stars and Active Galaxies, Oxford University Press Inc., NY, p. 469
Conway J.E. 1998, In: Zensus J.A., Taylor G.B., Wrobel J.M. (eds.) Radio Emission from Galactic and Extragalactic Compact Sources, IAU Coll. 164, ASP, San Francisco, p. 231
Dickey J.M., Salpeter E.E., Terzian Y. 1978, ApJS 36, 77
Gallimore J.F., Holloway A.J., Pedlar A., et al. 1998, A&A 333, 13
Gallimore J.F., Baum S.A., O'Dea C.P., et al. 1999, ApJ 524, 684
Gardner F.F., Whiteoak J.B. 1986, MNRAS 221, 537
Gardner F.F., Whiteoak J.B., Norris R.P., et al. 1992, MNRAS 258, 296
Hagiwara Y. 1998, PhD thesis, The Graduate University for Advanced studies, Nobeyama Radio Observatory
Hagiwara Y., Kohno K., Kawabe R., et al. 1997, PASJ 49, 171
Jaffe W., Ford H.C., Ferrarese L., et al. 1993, Nat 364, 213
Koribalski B. 1996, In: Skillman E.D. (ed.) The Minnesota lectures on Extragalactic Neutral Hydrogen, ASP, San Francisco, p. 238
Liszt H., Lucas R. 1996, A&A 314, 917
Liszt H.S., van der Hulst J.M., Burton W.B., et al. 1983, A&A 126, 341
Maloney P.R., Hollenbach D.J., Tielens A.G.G.M. 1996, ApJ 466, 561
Mebold U., Winnberg A., Kalberla P.M.W., et al. 1981, A&AS 46, 389
Miyoshi M., Moran J., Herrnstein J., et al. 1995, Nat 373, 127
Neufeld D.A., Maloney P.R. 1995, ApJ 447, L17
Pedlar A., Mundell C.G., Gallimore J.F., et al. 1996, Vistas in Astronomy 40, 91
Risaliti G., Maiolino R., Salvati M. 1999, ApJ 522, 157
Schmelz J.T., Baan W.A., Haschick A.D. 1987, ApJ 320, 145
Surace J.A., Mazzarella J., Soifer B.T., et al. 1993, AJ 105, 864